Chapter 2

Investigation of interactions among collinear Griffith cracks situated in a functionally graded medium under thermo-mechanical loading

2.1 Introduction

It is challenging to meet extremely desirable design requirements, such as high heat and corrosion resistance, sufficient high strength at elevated temperature, high resistance to wear, and required toughness in load-bearing elements, in this era of highly demanding technologies by using homogeneous materials. Metals and their alloys easily oxidize at high temperatures and typically lose their structural integrity. So, to get around this issue, coating or layering of different materials is employed. Composites made of metal or ceramic are typically suitable for coating or layering of materials. The oxidation and low toughness of composites at high temperatures are their major drawbacks. In contrast, ceramic coatings have a tendency to crack

because of their weaker interfacial bonding, high thermal stresses, and lower toughness.

Functionally graded materials (FGMs) were originally introduced by Japanese researchers in the 1980s while working on their aerospace projects for the requirements of the thermal barrier with the outside and inner temperatures of 2000 K and 1000 K respectively within 10 mm thickness [87]. FGMs are thought of as composites made up of two phases. These are synthesized so that the volume fractions of the elements vary continually to obtain a predefined composition profile. The composition profile ranges from 0% ceramic to 100% from the interface to the surface. The desired thermo-mechanical property determines the composition profile to be used. FGMs seem to hold great potential for a range of thermal shielding applications, including micro-electronics, furnace liners, high-temperature chambers, gas turbines, and space structures.

The failure of FGMs due to fracture is a significant issue that needs to be addressed. Various types of cracks can develop in FGMs when subjected to high-temperature loading conditions. In [33], some fundamental ideas of FGMs and their fracture-related issues were covered. [64] and [88] have demonstrated that, in contrast to other singularities found in a homogeneous medium, embedded cracks in non-homogeneous media possess the conventional square-root singularity. For FGMs subject to thermal, mechanical, and thermo-mechanical loads, several problems have previously been solved. In [88], an embedded crack that was parallel to the free surface and subject to continuously varying thermal characteristics in an infinite FGM media was examined. The crack surface was exposed to a steady-state heat flux. The same problem was extended by [8] for a partially insulated crack when the heating source is situated far from the crack zone, and a crack-closure algorithm is also discussed there.

When studying the fundamental crack issues in graded materials, crack interaction is a crucial component that must be taken into account. [24, 25, 26, 27, 57, 75] has done substantial research on crack interaction issues in homogeneous materials for a variety of crack configurations under different loadings. The interaction of cracks in homogenous materials may result in a rise in the magnitude of the stress intensity factors (SIFs). The outcome of FGMs, however, may be influenced by the locations of cracks, the direction of a material's property variation, and the relative dimensions [89, 93]. As a result, geometry plays a significant part in the fracture mechanics of FGMs. In [93], the problem of collinear cracks in an inhomogeneous orthotropic medium under mode I plane strain and plane stress loading conditions were investigated for cracks positioned in a plane and parallel to the direction of material property variations under external loads. The problem of collinear cracks in FGMs under thermal loading was researched in [89]. The article [94] investigates the thermal fracture problem for a functionally graded strip and an analytical model is developed for collinear cracks utilizing the piezoelectric model and steady-state temperature field. The interaction between a system of edge cracks in a functionally graded coating on a homogeneous substrate has been studied in [95].

Three collinear Griffith cracks are considered in this chapter in an infinite functionally graded medium along the x-axis. One of the cracks is in the middle, and the other two are symmetrically positioned on either side of it (see Figure 2.1). Steady-state heat flux is applied in the y-direction away from the location of these partially insulated cracks' region. Collinear cracks are subjected to mechanical stresses in the form of crack surface tractions. The material properties are assumed to vary in a direction perpendicular to the cracks' plane and are represented by exponential functions. The medium being addressed here can be thought of as a non-homogeneous elastic one under the condition of plane strain or plane stress.

Here, the coupling effects between mechanical and thermal loadings are not taken into account as the isotropic stress-strain law is followed. Equations for elasticity and heat conduction are solved using the Fourier sine and cosine transforms and the superposition concept. These equations are analytically reduced to a set of first-order integral equations. These sets of integral equations are solved numerically to produce temperature and displacement fields in the medium under thermal and mechanical loading. The thermal crack surface stresses are also determined. Calculations are made for particular cases of thermal, mechanical, and combined mechanical and thermal loadings to determine mode I SIFs and stress magnification factors (SMFs). The numerical computation and pictorial representations of the SMFs to find the possibilities of shielding and amplification of the cracks are the key features of the present chapter.

2.2 Mathematical formulation of the problem

2.2.1 Schematic description

Consider an unbounded medium ($-\infty < x < \infty, -\infty < y < \infty$) with a central and two outer partially insulated Griffith cracks that are symmetrically positioned along the x-axis and have lengths $2a$ and c-b respectively (see Figure 2.1).

The material property gradient is directed in the y-direction. It is assumed that Poisson's ratio v is constant [28, 38]. Other thermo-mechanical properties depend on the y-coordinate only. Using exponential functions, they are expressed as

$$k = k_0 \exp(\delta y), \quad \mu = \mu_0 \exp(\beta y), \quad \alpha = \alpha_0 \exp(\gamma y), \tag{2.1}$$

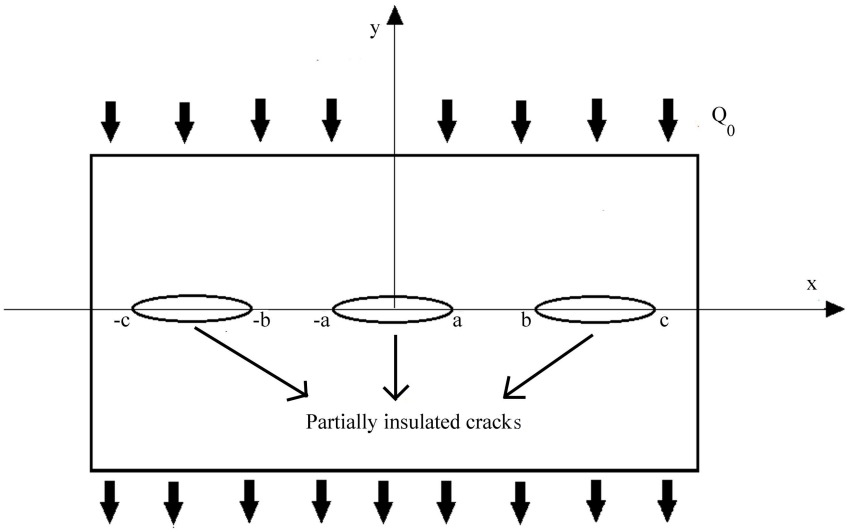

Figure 2.1: Schematic diagram of the problem.

where k, μ, and α are the coefficients of heat conductivity, shear modulus, and thermal expansion respectively, and k_0, μ_0 and α_0 correspond to the initial values of k, μ, and α, respectively, along the crack plane. δ, β and γ are the nonhomogeneity parameters. These, in turn, control variations in thermal expansion coefficient, shear modulus, and heat conductivity, respectively. Two different types of loading are taken into account in the mathematical model. The first is a steady-state heat flux that is applied in the y-direction away from the crack region, and the second is arbitrary crack surface tractions described in terms of external mechanical loads.

2.2.2 Governing equations and boundary conditions

In the Cartesian coordinate system (x, y), the x and y components of the displacement field are u and ν, the stress field components are σ_{xx}, σ_{yy} and σ_{xy}, the strain field components are $\epsilon_{xx}, \epsilon_{yy}$ and ϵ_{xy} and the temperature field is T.

The model under consideration is symmetric about the y-axis. As a result, the region is considered as $0 \leq x < \infty, -\infty < y < +\infty$. The heat equation and corresponding boundary conditions [8, 65] are given by

$$\nabla^2 T + \delta \frac{\partial T}{\partial y} = 0, \tag{2.2}$$

$$k\frac{\partial T(x,y)}{\partial y} = Q_0, \qquad y \to \pm\infty,\ 0 \leq x < \infty, \tag{2.3}$$

$$k_0\frac{\partial T(x,0^+)}{\partial y} = k_0\frac{\partial T(x,0^-)}{\partial y} = k^* Q_0, \qquad 0 \leq x \leq a,\ b \leq x \leq c, \tag{2.4}$$

$$T(x,0^+) = T(x,0^-), \qquad \frac{\partial T(x,0^+)}{\partial y} = \frac{\partial T(x,0^-)}{\partial y}, \quad a < x < b,\ x > c, \tag{2.5}$$

where Q_0 is the heat flux corresponding to the perfect conduction case and k^* is a constant heat conductivity index ranging from 0 to 1. k^*= 0 corresponds to perfect insulation and k^*=1 corresponds to perfect conduction along the cracked surface. It is evident from the equation (2.3) that the flux is applied away from the crack region. The partial insulation of the crack surfaces is described by equation (2.4). It is assumed that the cracks allow some heat flux Q_y, where Q_y is only a certain percentage of Q_0. Continuity of temperature field and heat flux are shown through equation (2.5).

The following equations give the continuity of displacements under plane elasticity [8]

$$(k+1)\frac{\partial^2 u}{\partial x^2} + (k-1)\frac{\partial^2 u}{\partial y^2} + 2\frac{\partial^2 \nu}{\partial x \partial y} + \beta(k-1)\frac{\partial u}{\partial y} + \beta(k-1)\frac{\partial \nu}{\partial y} = 4\alpha_0 \exp(\gamma y)\frac{\partial T}{\partial x}, \tag{2.6}$$

$$(k-1)\frac{\partial^2 \nu}{\partial x^2} + (k+1)\frac{\partial^2 \nu}{\partial y^2} + 2\frac{\partial^2 u}{\partial x \partial y} + \beta(3-k)\frac{\partial u}{\partial x} + \beta(k+1)\frac{\partial \nu}{\partial y} = 4\alpha_0 \exp(\gamma y)\left[(\beta+\gamma)T + \frac{\partial T}{\partial y}\right], \tag{2.7}$$

under the boundary conditions

$$\sigma_{xy}(x,0^+) = \sigma_{xy}(x,0^-) = w_1^M(x), \qquad 0 \le x \le a,\ b \le x \le c, \tag{2.8}$$

$$\sigma_{yy}(x,0^+) = \sigma_{yy}(x,0^-) = w_2^M(x), \qquad 0 \le x \le a,\ b \le x \le c, \tag{2.9}$$

$$\sigma_{xy}(x,y) = \sigma_{yy}(x,y) = 0, \qquad y \to \pm\infty,\ 0 \le x < \infty, \tag{2.10}$$

$$\sigma_{xy}(x,0^+) = \sigma_{xy}(x,0^-), \qquad \sigma_{yy}(x,0^+) = \sigma_{yy}(x,0^-), \quad a < x < b,\ x > c, \tag{2.11}$$

$$u(x,0^+) = u(x,0^-), \qquad \nu(x,0^+) = \nu(x,0^-), \qquad a < x < b,\ x > c, \tag{2.12}$$

where k is $(3-4v)$ for plane strain and $(3-v)/(1+v)$ for generalized plane stress. Equations (2.8) and (2.9) take into account the applied tangential and normal crack surface tractions as $w_1^M(x)$ and $w_2^M(x)$, respectively. These are essentially given in terms of the external mechanical loads. Employing Hooke's law the stress components [12] can be expressed as

$$\sigma_{xx} = \frac{\mu}{k-1}\left[(k+1)\frac{\partial u}{\partial x} + (3-k)\frac{\partial \nu}{\partial y} - 4\alpha_0 T\right], \tag{2.13}$$

$$\sigma_{yy} = \frac{\mu}{k-1}\left[(3-k)\frac{\partial u}{\partial x} + (k+1)\frac{\partial \nu}{\partial y} - 4\alpha_0 T\right], \tag{2.14}$$

$$\sigma_{xy} = \mu\left[\frac{\partial u}{\partial y} + \frac{\partial \nu}{\partial x}\right]. \tag{2.15}$$

2.3 Solution of temperature field

Employing the superposition method, the temperature field can be expressed as [58]

$$T(x,y) = T_1(y) + T_2(x,y), \tag{2.16}$$

where $T_1(y)$ and $T_2(x,y)$ represent the temperature fields of the uncracked and cracked mediums, respectively.

For $T_1(y)$, the governing equation and related boundary conditions are

$$\frac{d^2T_1}{dy^2} + \delta\frac{dT_1}{dy} = 0, \tag{2.17}$$

$$\frac{\partial T_1(y)}{\partial y} = \frac{Q_0}{k_0}\exp(-\delta y), \qquad y \to \pm\infty, \quad 0 \le x < \infty. \tag{2.18}$$

For $T_2(x, y)$, the governing equation and related boundary conditions are given by

$$\nabla^2 T_2 + \delta\frac{\partial T_2}{\partial y} = 0, \tag{2.19}$$

$$\frac{\partial T_2(x,y)}{\partial y} = 0, \qquad y \to \pm\infty,\ 0 \le x < \infty, \tag{2.20}$$

$$\frac{\partial T_2(x,0^+)}{\partial y} = \frac{\partial T_2(x,0^-)}{\partial y} = (k^* - 1)\frac{dT_1(0)}{dy}, \qquad 0 \le x \le a,\ b \le x \le c, \tag{2.21}$$

$$T_2(x,0^+) = T_2(x,0^-), \quad \frac{\partial T_2(x,0^+)}{\partial y} = \frac{\partial T_2(x,0^-)}{\partial y},\ a < x < b,\ x > c, \tag{2.22}$$

For $T_1(0) = 0$ [9], the following solution for $T_1(y)$ is expressed as

$$T_1(y) = \frac{Q_0}{k_0\delta}\left(1 - \exp(-\delta y)\right). \tag{2.23}$$

The application of Fourier cosine transform in equation (2.19) gives

$$T_2(x,y) = \begin{cases} \frac{(1-k^*)Q_0}{k_0}\int_0^\infty \left[\left(A_1(\rho)\,\exp(n_1 y) + A_2(\rho)\,\exp(n_2 y)\right)\cos(\rho x)d\rho\right], & y > 0, \\ \frac{(1-k^*)Q_0}{k_0}\int_0^\infty \left[\left(A_3(\rho)\,\exp(n_1 y) + A_4(\rho)\,\exp(n_2 y)\right)\cos(\rho x)d\rho\right], & y < 0, \end{cases} \tag{2.24}$$

where A_k $(k = 1, 2, 3, 4)$ are arbitrary unknown functions in ρ and n_i $(i = 1, 2)$ are the roots of the characteristic equation given by

$$n^2 + \delta n - \rho^2 = 0, \tag{2.25}$$

$$\text{as } n_1 = \frac{1}{2}\left(-\delta + \sqrt{\delta^2 + 4\rho^2}\right) \text{ and } n_2 = \frac{1}{2}\left(-\delta - \sqrt{\delta^2 + 4\rho^2}\right). \tag{2.26}$$

Observing that $n_1 > 0$ and $n_2 < 0$ and using boundary conditions (2.20), we have

$$A_1(\rho) = 0,\ A_4(\rho) = 0.$$

Thus (2.24) reduces to

$$T_2(x,y) = \begin{cases} \frac{(1-k^*)Q_0}{k_0} \int_0^\infty \left[A_2(\rho)\ \exp(n_2 y)\cos(\rho x)d\rho\right], & y > 0, \\ \frac{(1-k^*)Q_0}{k_0} \int_0^\infty \left[A_3(\rho)\ \exp(n_1 y)\cos(\rho x)d\rho\right], & y < 0. \end{cases} \tag{2.27}$$

Define an unknown function as

$$\psi(x) = \frac{\partial}{\partial x}\left[T(x,0^+) - T(x,0^-)\right]. \tag{2.28}$$

From (2.22) and (2.23), it is evident that

$$\psi(x) = \frac{\partial}{\partial x}\left[T_2(x,0^+) - T_2(x,0^-)\right], \tag{2.29}$$

$$\int_0^a \psi(t)dt + \int_b^c \psi(t)dt = 0, \quad \psi(x) = 0, \qquad a < x < b, \quad x > c. \tag{2.30}$$

Using (2.21), (2.22), (2.27) and (2.29), $A_2(\rho)$ and $A_3(\rho)$ can be written in terms of ψ as

$$A_2(\rho) = \frac{2n_1k_0}{\pi\rho(n_2-n_1)(1-k^*)Q_0}\left[\int_0^a \psi(t)\sin(\rho t)dt + \int_b^c \psi(t)\sin(\rho t)dt\right], \tag{2.31}$$

$$A_3(\rho) = \frac{2n_2k_0}{\pi\rho(n_2-n_1)(1-k^*)Q_0}\left[\int_0^a \psi(t)\sin(\rho t)dt + \int_b^c \psi(t)\sin(\rho t)dt\right]. \tag{2.32}$$

2.3.1 Numerical solution of integral equation related to temperature field

The boundary condition (2.21) with the aid of (2.32) yields the following singular integral equation [44]

$$\int_0^a \left[k(x,t)+\frac{1}{t-x}+\frac{1}{t+x}\right]\psi(t)dt+\int_b^c \left[k(x,t)+\frac{1}{t-x}+\frac{1}{t+x}\right]\psi(t)dt = \frac{2\pi(k^*-1)Q_0}{k_0}, \qquad 0\le x\le a, \quad b\le x\le c, \tag{2.33}$$

where $k(x,t)$ is a Fredholm kernel given in equation (A.0.1) in Appendix A. The integration interval in the singular term of the first term of the left-hand side of the equation (2.33) can be extended from $[0,a]$ to $[-a,a]$ by using the symmetry property which shows that $\psi(x)$ becomes an odd function in $[-a,a]$ and equation (2.33) takes the form

$$\int_{-a}^a \frac{\psi(t)}{t-x}dt+\int_0^a k(x,t)\psi(t)dt+\int_b^c \left[k(x,t)+\frac{1}{t-x}+\frac{1}{t+x}\right]\psi(t)dt = \frac{2\pi(k^*-1)Q_0}{k_0}, \qquad 0\le x\le a, \quad b\le x\le c. \tag{2.34}$$

To solve the singular integral equation (2.34), let us define the parameters as [93]

$$\eta_1=\frac{t}{a}, \quad \xi_1=\frac{x}{a}, \quad \eta_2=\frac{2t-(b+c)}{c-b}, \quad \xi_2=\frac{2x-(b+c)}{c-b}, \tag{2.35}$$

$$\psi(t)=\begin{cases}\psi_1(\eta_1), & -1\le\eta_1\le 1,\\ \psi_2(\eta_2), & -1\le\eta_2\le 1.\end{cases} \tag{2.36}$$

With the aid of (2.35), (2.36), [32, 61], the integral equation (2.34) reduces to

$$\int_{-1}^1 \frac{\psi_1(\eta_1)}{\eta_1-\xi_1}d\eta_1+\int_0^1 k_{11}(\xi_1,\eta_1)\psi_1(\eta_1)d\eta_1+\int_{-1}^1 \left[k_{12}(\xi_1,\eta_2)+\frac{1}{\eta_2-z_{12}(\xi_1)}\right.$$

$$+\frac{1}{\eta_2-g_{12}(\xi_1)}\Bigg]\psi_2(\eta_2)d\eta_2=\frac{2\pi(k^*-1)Q_0}{k_0},\qquad -1\le\xi_1\le 1, \tag{2.37}$$

$$\int_{-1}^{1}\frac{\psi_1(\eta_1)}{\eta_1-z_{21}(\xi_2)}d\eta_1+\int_0^1 k_{21}(\xi_2,\eta_1)\psi_1(\eta_1)d\eta_1\int_{-1}^{1}\Bigg[k_{22}(\xi_2,\eta_2)+\frac{1}{\eta_2-\xi_2}$$
$$+\frac{1}{\eta_2-g_{22}(\xi_2)}\Bigg]\psi_2(\eta_2)d\eta_2=\frac{2\pi(k^*-1)Q_0}{k_0},\qquad -1\le\xi_2\le 1, \tag{2.38}$$

where $k_{ij}(\xi_i,\eta_j)$ $(i,j=1,2)$, $g_{12}(\xi_1)$, $g_{22}(\xi_2)$, $z_{12}(\xi_1)$ and $z_{21}(\xi_2)$ are defined in Appendix A (A.0.2-A.0.9) and $\psi_i(\eta_i)$ $(i=1,2)$ satisfy the following conditions

$$\int_{-1}^{1}\psi_1(\eta_1)d\eta_1=0,\qquad \int_{-1}^{1}\psi_2(\eta_2)d\eta_2=0. \tag{2.39}$$

The system of integral equations (2.37) and (2.38) can be solved by using truncated series of Chebyshev polynomials of the first kind T_n [36] by expressing

$$\psi_1(\eta_1)=\frac{Q_0}{k_0}\sum_{n=1}^{M1}\frac{a_{1n}\,T_n(\eta_1)}{\sqrt{1-\eta_1^2}},\qquad \psi_2(\eta_2)=\frac{Q_0}{k_0}\sum_{n=1}^{M2}\frac{a_{2n}\,T_n(\eta_2)}{\sqrt{1-\eta_2^2}}, \tag{2.40}$$

where a_{1n} and a_{2n} are unknown dimensionless constants. Equations (2.37) and (2.38) are reduced to an algebraic system in $a_{11},...,a_{1M1}$, $a_{21},...,a_{2M2}$ utilizing (2.40), (A.0.10) (in Appendix A) and collocation technique [37]. The temperature distributions can be obtained for all the three collinear cracks by solving the system numerically.

2.4 Solution of displacement field

Employing Fourier sine transform in equation (2.6), Fourier cosine transform in equations (2.7) and (2.27), the expressions of displacement field are found as

$$u(x,y)=\begin{cases}\int_0^\infty \left[\sum_{k=1}^4 c_k(\rho)\,\exp(m_k y)\right]\sin(\rho x)d\rho \\ \quad +\frac{(1-k^*)Q_0\alpha_0}{k_0}\int_0^\infty \left[\frac{\zeta_1(\rho)}{d_1(\rho)}\,\exp\left((\gamma+n_2)y\right)\right]\sin(\rho x)d\rho, & y>0,\\ \int_0^\infty \left[\sum_{k=1}^4 c_{k+4}(\rho)\,\exp(m_k y)\right]\sin(\rho x)d\rho \\ \quad +\frac{(1-k^*)Q_0\alpha_0}{k_0}\int_0^\infty \left[\frac{\zeta_3(\rho)}{d_2(\rho)}\,\exp\left((\gamma+n_1)y\right)\right]\sin(\rho x)d\rho, & y<0,\end{cases} \tag{2.41}$$

$$\nu(x,y)=\begin{cases}\int_0^\infty \left[\sum_{k=1}^4 c_k(\rho)s_k(\rho)\,\exp(m_k y)\right]\cos(\rho x)d\rho \\ \quad +\frac{(1-k^*)Q_0\alpha_0}{k_0}\int_0^\infty \left[\frac{\zeta_2(\rho)}{d_1(\rho)}\exp\left((\gamma+n_2)y\right)\right]\cos(\rho x)d\rho \\ \quad +\frac{4\alpha_0 Q_0}{\delta(k+1)k_0}\left[\frac{\exp(\gamma y)}{\gamma}-\frac{\exp((\gamma-\delta)y)}{(\gamma-\delta)}\right], & y>0,\\ \int_0^\infty \left[\sum_{k=1}^4 c_{k+4}(\rho)s_k(\rho)\,\exp(m_k y)\right]\cos(\rho x)d\rho \\ \quad +\frac{(1-k^*)Q_0\alpha_0}{k_0}\int_0^\infty \left[\frac{\zeta_4(\rho)}{d_2(\rho)}\exp\left((\gamma+n_1)y\right)\right]\cos(\rho x)d\rho \\ \quad +\frac{4\alpha_0 Q_0}{\delta(k+1)k_0}\left[\frac{\exp(\gamma y)}{\gamma}-\frac{\exp((\gamma-\delta)y)}{(\gamma-\delta)}\right], & y<0,\end{cases} \tag{2.42}$$

where $m_i (i=1,...,4)$ are the roots of the following characteristic equation

$$m^4+2\beta m^3+(\beta^2-2\rho^2)m^2-2\beta\rho^2 m+\left(\rho^4+\rho^2\beta^2 f_0^2\right)=0, \tag{2.43}$$

$$\text{as } m_1=\bar{m}_3=\frac{1}{2}\left[-\beta+\sqrt{\beta^2+4\rho^2+4i\rho\beta f_0}\right] \text{ and}$$

$$m_2=\bar{m}_4=\frac{1}{2}\left[-\beta-\sqrt{\beta^2+4\rho^2+4i\rho\beta f_0}\right], \tag{2.44}$$

and c_k $(k=1,...,8)$ are arbitrary unknown functions in ρ, s_i $(i=1,...,4)$, d_i $(i=1,2)$, ζ_i $(i=1,...,4)$ are given in Appendix A (A.0.11-A.0.17) and $f_0=\sqrt{(3-k)/(1+k)}$. Observe that $\Re(m_1,m_3)>0$, $\Re(m_2,m_4)<0$ and using boundary conditions (2.10), we have

$$c_1(\rho)=0,\ c_3(\rho)=0,\ c_6(\rho)=0,\ c_8(\rho)=0.$$

Thus, (2.41) and (2.42) reduce to

$$u(x,y)=\begin{cases}\int_0^\infty \left[c_2(\rho)\,\exp(m_2y)+c_4(\rho)\,\exp(m_4y)\right]\sin(\rho x)d\rho \\ \quad+\frac{(1-k^*)Q_0\alpha_0}{k_0}\int_0^\infty\left[\frac{\zeta_1(\rho)}{d_1(\rho)}\,\exp\left((\gamma+n_2)y\right)\right]\sin(\rho x)d\rho, \quad y>0,\\ \int_0^\infty \left[c_5(\rho)\,\exp(m_1y)+c_7(\rho)\,\exp(m_3y)\right]\sin(\rho x)d\rho \\ \quad+\frac{(1-k^*)Q_0\alpha_0}{k_0}\int_0^\infty\left[\frac{\zeta_3(\rho)}{d_2(\rho)}\,\exp\left((\gamma+n_1)y\right)\right]\sin(\rho x)d\rho, \quad y<0,\end{cases} \tag{2.45}$$

$$\nu(x,y)=\begin{cases}\int_0^\infty \left[c_2(\rho)s_2(\rho)\,\exp(m_2y)+c_4(\rho)s_4(\rho)\,\exp(m_4y)\right]\cos(\rho x)d\rho \\ \quad+\frac{(1-k^*)Q_0\alpha_0}{k_0}\int_0^\infty\left[\frac{\zeta_2(\rho)}{d_1(\rho)}\exp((\gamma+n_2)y)\right]\cos(\rho x)d\rho \\ \quad+\frac{4\alpha_0Q_0}{\delta(k+1)k_0}\left[\frac{\exp(\gamma y)}{\gamma}-\frac{\exp((\gamma-\delta)y)}{(\gamma-\delta)}\right], & y>0,\\ \int_0^\infty \left[c_5(\rho)s_1(\rho)\,\exp(m_1y)+c_7(\rho)s_3(\rho)\,\exp(m_3y)\right]\cos(\rho x)d\rho \\ \quad+\frac{(1-k^*)Q_0\alpha_0}{k_0}\int_0^\infty\left[\frac{\zeta_4(\rho)}{d_2(\rho)}\exp((\gamma+n_1)y)\right]\cos(\rho x)d\rho \\ \quad+\frac{4\alpha_0Q_0}{\delta(k+1)k_0}\left[\frac{\exp(\gamma y)}{\gamma}-\frac{\exp((\gamma-\delta)y)}{(\gamma-\delta)}\right], & y<0.\end{cases} \tag{2.46}$$

Introducing two unknown functions ψ_u and ψ_ν as

$$\psi_u(x)=\frac{\partial}{\partial x}\left[u(x,0^+)-u(x,0^-)\right], \quad \psi_\nu(x)=\frac{\partial}{\partial x}\left[\nu(x,0^+)-\nu(x,0^-)\right]. \tag{2.47}$$

It follows from (2.12) that

$$\int_0^a\psi_u(t)dt+\int_b^c\psi_u(t)dt=0, \qquad \psi_u(x)=0, \qquad a<x<b, \quad x>c, \tag{2.48}$$

$$\int_0^a\psi_\nu(t)dt+\int_b^c\psi_\nu(t)dt=0, \qquad \psi_\nu(x)=0, \qquad a<x<b \quad x>c. \tag{2.49}$$

With the aid of (2.11-2.15), (2.45-2.49) four equations are found which can be written in the matrix form as

$$\begin{bmatrix} q_2 & q_4 & -q_1 & -q_3 \\ p_2 & p_4 & -p_1 & -p_3 \\ 1 & 1 & -1 & -1 \\ s_2 & s_4 & -s_1 & -s_3 \end{bmatrix} \begin{bmatrix} c_2(\rho) \\ c_4(\rho) \\ c_5(\rho) \\ c_7(\rho) \end{bmatrix} = \begin{bmatrix} e_1(\rho) \\ e_2(\rho) \\ f_1(\rho) + f_{11}(\rho) \\ f_2(\rho) + f_{22}(\rho) \end{bmatrix}, \tag{2.50}$$

where $p_k\,(k = 1, ..., 4)$, $q_k\,(k = 1, ..., 4)$, $e_k\,(k = 1, 2)$, $f_k\,(k = 1, 2)$ and $f_{kk}\,(k = 1, 2)$ are functions of ρ and given in Appendix A (A.0.18 - A.0.25). With the help of (2.50), $c_i(\rho)\,(i = 2, 4, 5, 7)$ can be expressed in terms of ψ_u and ψ_ν.

2.4.1 Numerical solution of integral equations related to stress field

The boundary conditions (2.8) and (2.9) yield two singular integral equations which after using the symmetry property reduce to

$$\int_0^a k_{u1}(x,t)\,\psi_u(t)dt + \int_{-a}^{+a} \frac{\psi_u(t)}{t-x}dt + \int_b^c \left[k_{u1}(x,t) + \frac{1}{t-x} - \frac{1}{t+x}\right]\psi_u(t)dt$$
$$+ \int_0^a k_{\nu 1}(x,t)\,\psi_\nu(t)dt \; + \frac{\beta}{2}\int_{-a}^{+a} \log|t-x|\,\psi_\nu(t)dt + \int_b^c \left[k_{v1}(x,t) + \frac{\beta}{2}\log\left|\frac{t-x}{t+x}\right|\right]$$
$$\psi_\nu(t)dt = w_1(x), \qquad 0 \le x \le a, \quad b \le x \le c, \tag{2.51}$$
$$\int_0^a k_{u2}(x,t)\,\psi_u(t)dt - \frac{\beta}{2}\int_{-a}^{+a} \log|t-x|\,\psi_u(t)dt + \int_b^c \left[k_{u2}(x,t) - \frac{\beta}{2}\log|(t-x)(t+x)|\right]$$
$$\psi_u(t)dt + \int_0^a k_{\nu 2}(x,t)\,\psi_\nu(t)dt + \int_{-a}^{+a} \frac{\psi_\nu(t)}{t-x}dt + \int_b^c \left[k_{\nu 2}(x,t) + \frac{1}{t-x} + \frac{1}{t+x}\right]\psi_\nu(t)dt$$
$$= w_2(x), \qquad 0 \le x \le a,\; b \le x \le c, \tag{2.52}$$

where the known functions $k_{ui}\,(x,t)\,(i = 1, 2)$, $k_{\nu i}\,(x,t)\,(i = 1, 2)$ are Fredholm kernels given by equations (A.0.26-A.0.29) of Appendix A. Expressions of $w_i(x)\,(i =$

1, 2) are given by

$$w_1(x) = \frac{\pi(1+k)}{2\mu_0}\left[w_1^M(x) + w_1^T(x)\right], \tag{2.53}$$

$$w_2(x) = \frac{\pi(1+k)}{2\mu_0}\left[w_2^M(x) + w_2^T(x)\right], \tag{2.54}$$

$$w_1^T(x) = \mu_0 \int_0^\infty \left[g_1 e_1 + g_2 e_2 + g_3 f_{11} + g_4 f_{22} + g_5\right] \sin(\rho x) d\rho, \tag{2.55}$$

$$w_2^T(x) = \frac{\mu_0}{k-1} \int_0^\infty \left[h_1 e_1 + h_2 e_2 + h_3 f_{11} + h_4 f_{22} + h_5\right] \cos(\rho x) d\rho, \tag{2.56}$$

e_i $(i = 1, 2)$, f_{ii} $(i = 1, 2)$, g_i $(i = 1, ..., 4)$, h_i $(i = 1, ..., 4)$ are given in Appendix A (A.0.20 - A.0.21, A.0.24 - A.0.25, A.0.35 - A.0.43), $w_1^T(x)$ and $w_2^T(x)$ are thermal tangential and normal stresses applied on the crack surface, respectively and depend on the temperature and parameters δ, β and γ.

Using the (2.35) [32, 61], the integral equations (2.51) and (2.52) become

$$\begin{aligned}
&\int_0^1 k_{u11}(\xi_1, \eta_1)\, \psi_{u1}(\eta_1) d\eta_1 + \int_{-1}^1 \frac{\psi_{u1}(\eta_1)}{\eta_1 - \xi_1} d\eta_1 + \int_{-1}^1 \left[k_{u12}(\xi_1, \eta_2) + \frac{1}{\eta_2 - z_{12}(\xi_1)}\right. \\
&\left. - \frac{1}{\eta_2 - g_{12}(\xi_1)}\right] \psi_{u2}(\eta_2) d\eta_2 + \int_0^1 k_{\nu 11}(\xi_1, \eta_1)\, \psi_{\nu 1}(\eta_1) d\eta_1 + \frac{\beta a}{2} \int_{-1}^1 \log|a(\eta_1 - \xi_1)| \\
&\times \psi_{\nu 1}(\eta_1) d\eta_1 + \int_{-1}^1 \left[k_{\nu 12}(\xi_1, \eta_2) + \frac{\beta(c-b)}{4} \log\left|\frac{\eta_2 - z_{12}(\xi_1)}{\eta_2 - g_{12}(\xi_1)}\right|\right] \psi_{\nu 2}(\eta_2) d\eta_2 \\
&= w_1(\xi_1), \qquad -1 \le \xi_1 \le 1,
\end{aligned} \tag{2.57}$$

$$\begin{aligned}
&\int_0^1 k_{u21}(\xi_2, \eta_1)\, \psi_{u1}(\eta_1) d\eta_1 + \int_{-1}^1 \frac{\psi_{u1}(\eta_1)}{\eta_1 - z_{21}(\xi_2)} d\eta_1 + \int_{-1}^1 \left[k_{u22}(\xi_2, \eta_2) + \frac{1}{\eta_2 - \xi_2}\right. \\
&\left. - \frac{1}{\eta_2 - g_{22}(\xi_2)}\right] \psi_{u2}(\eta_2) d\eta_2 + \int_0^1 k_{\nu 21}(\xi_2, \eta_1)\, \psi_{\nu 1}(\eta_1) d\eta_1 + \frac{\beta a}{2} \int_{-1}^1 \log|a(\eta_1 - z_{21}(\xi_2))| \\
&\times \psi_{\nu 1}(\eta_1) d\eta_1 + \int_{-1}^1 \left[k_{\nu 22}(\xi_2, \eta_2) + \frac{\beta(c-b)}{4} \log\left|\frac{\eta_2 - \xi_2}{\eta_2 - g_{22}(\xi_2)}\right|\right] \psi_{\nu 2}(\eta_2) d\eta_2 \\
&= w_1(\xi_2), \qquad -1 \le \xi_2 \le 1,
\end{aligned} \tag{2.58}$$

$$\begin{aligned}
&\int_0^1 k_{u31}(\xi_1, \eta_1)\, \psi_{u1}(\eta_1) d\eta_1 - \frac{\beta a}{2} \int_{-1}^1 \log|a(\eta_1 - \xi_1)|\, \psi_{u1}(\eta_1) d\eta_1 + \int_{-1}^1 \left[k_{u32}(\xi_1, \eta_2)\right. \\
&\left. - \frac{\beta(c-b)}{4} \log\left|\left(\frac{c-b}{2}\right)^2 (\eta_2 - z_{12}(\xi_1))\,(\eta_2 - g_{12}(\xi_1))\right|\right] \psi_{u2}(\eta_2) d\eta_2 + \int_0^1 k_{\nu 31}(\xi_1, \eta_1)
\end{aligned}$$

$$\times \psi_{\nu 1}(\eta_1)d\eta_1 + \int_{-1}^{1} \frac{\psi_{\nu 1}(\eta_1)}{\eta_1 - \xi_1} d\eta_1 + \int_{-1}^{1} \left[k_{\nu 32}(\xi_1, \eta_2) + \frac{1}{\eta_2 - z_{12}(\xi_1)} + \frac{1}{\eta_2 - g_{12}(\xi_1)} \right]$$

$$\times \psi_{\nu 2}(\eta_2)d\eta_2 = w_2(\xi_1), \qquad -1 \le \xi_1 \le 1, \tag{2.59}$$

$$\int_0^1 k_{u41}(\xi_2, \eta_1)\, \psi_{u1}(\eta_1)d\eta_1 - \frac{\beta a}{2} \int_{-1}^{1} \log\left|a(\eta_1 - z_{21}(\xi_2))\right| \psi_{u1}(\eta_1)d\eta_1 + \int_{-1}^{1} \left[k_{u42}(\xi_2, \eta_2) \right.$$

$$\left. - \frac{\beta(c-b)}{4} \log \left| \left(\frac{c-b}{2} \right)^2 (\eta_2 - \xi_2)\, (\eta_2 - g_{22}(\xi_2)) \right| \right] \psi_{u2}(\eta_2)d\eta_2 + \int_0^1 k_{\nu 41}(\xi_2, \eta_1)$$

$$\times \psi_{\nu 1}(\eta_1)d\eta_1 + \int_{-1}^{1} \frac{\psi_{\nu 1}(\eta_1)}{\eta_1 - z_{21}(\xi_2)} d\eta_1 + \int_{-1}^{1} \left[k_{\nu 42}(\xi_2, \eta_2) + \frac{1}{\eta_2 - \xi_2} + \frac{1}{\eta_2 - g_{22}(\xi_2)} \right]$$

$$\times \psi_{\nu 2}(\eta_2)d\eta_2 = w_2(\xi_2), \qquad -1 \le \xi_2 \le 1, \tag{2.60}$$

where k_{uij} $(i = 1, ..., 4, j = 1, 2)$, $k_{\nu ij}$ $(i = 1, ..., 4, j = 1, 2)$, $g_{12}(\xi_1)$, $g_{22}(\xi_2)$, $z_{12}(\xi_1)$, $z_{21}(\xi_2)$ and $w_i(\xi_j)$ $(i, j = 1, 2)$ are given in Appendix A, with

$$\psi_u(t) = \begin{cases} \psi_{u1}(\eta_1), & -1 \le \eta_1 \le 1, \\ \psi_{u2}(\eta_2), & -1 \le \eta_2 \le 1, \end{cases} \qquad \psi_\nu(t) = \begin{cases} \psi_{\nu 1}(\eta_1), & -1 \le \eta_1 \le 1, \\ \psi_{\nu 2}(\eta_2), & -1 \le \eta_2 \le 1, \end{cases} \tag{2.61}$$

and $\psi_{u1}(\eta_1)$, $\psi_{u2}(\eta_2)$, $\psi_{\nu 1}(\eta_1)$ and $\psi_{\nu 2}(\eta_2)$ satisfy the following conditions

$$\int_{-1}^{1} \psi_{u1}(\eta_1)d\eta_1 = 0, \quad \int_{-1}^{1} \psi_{u2}(\eta_2)d\eta_2 = 0, \quad \int_{-1}^{1} \psi_{\nu 1}(\eta_1)d\eta_1 = 0, \quad \int_{-1}^{1} \psi_{\nu 2}(\eta_2)d\eta_2 = 0. \tag{2.62}$$

The system of integral equations (2.57-2.60) can be solved by using truncated series of Chebyshev polynomials of the first kind T_n by defining

$$\psi_{u1}(\eta_1) = \frac{\pi(1+k)Q_0\alpha_0}{2k_0} \sum_{n=1}^{N1} \frac{b1_n\, T_n(\eta_1)}{\sqrt{1-\eta_1^2}}, \qquad \psi_{u2}(\eta_2) = \frac{\pi(1+k)Q_0\alpha_0}{2k_0} \sum_{n=1}^{N2} \frac{b2_n\, T_n(\eta_2)}{\sqrt{1-\eta_2^2}},$$

$$\psi_{\nu 1}(\eta_1) = \frac{\pi(1+k)Q_0\alpha_0}{2k_0} \sum_{n=1}^{N3} \frac{c1_n\, T_n(\eta_1)}{\sqrt{1-\eta_1^2}}, \qquad \psi_{\nu 2}(\eta_2) = \frac{\pi(1+k)Q_0\alpha_0}{2k_0} \sum_{n=1}^{N4} \frac{c2_n\, T_n(\eta_2)}{\sqrt{1-\eta_2^2}},$$

where $b1_n, b2_n, c1_n$ and $c2_n$ are unknown dimensionless constants. Using (A.0.10) and collocation method [37], the equations (2.57-2.60) are converted to an algebraic system in $b1_1, ..., b1_{N1}$, $b2_1, ..., b2_{N2}$, $c1_1, ..., c1_{N3}$, $c2_1, ..., c2_{N4}$. Solving this system numerically the stress intensity factors at the crack tips can be determined using the expression of the displacement components.

2.5 Driving force parameters

The mode I crack tip stress intensity factors (SIFs) are defined as

$$K_I^a = \lim_{x \to a^+} \sqrt{2(x-a)}\sigma_{yy}(x,0), \tag{2.63}$$

$$K_I^b = \lim_{x \to b^-} \sqrt{2(b-x)}\sigma_{yy}(x,0), \tag{2.64}$$

$$K_I^c = \lim_{x \to c^+} \sqrt{2(x-c)}\sigma_{yy}(x,0). \tag{2.65}$$

The analytical expressions of SIFs in terms of the coefficients $c1_n$ and $c2_n$ ($n = 1, 2, ..., N_i; i = 3, 4$) [35, 92] can be found as

$$K_I^a = -\left(p_0\sqrt{a}\right)\sum_{n=1}^{N3} c1_n, \tag{2.66}$$

$$K_I^b = \left(p_0\sqrt{\frac{c-b}{2}}\right)\sum_{n=1}^{N4}(-1)^n c2_n, \tag{2.67}$$

$$K_I^c = -\left(p_0\sqrt{\frac{c-b}{2}}\right)\sum_{n=1}^{N4} c2_n, \tag{2.68}$$

where $p_0 = (\mu_0 Q_0 \alpha_0)/k_0$.

The mode I crack tip stress magnification factors (SMFs) are determined by

$$M_I^a = \frac{K_I^a}{K_{0I}^a}, \qquad M_I^b = \frac{K_I^b}{K_{0I}^b}, \qquad M_I^c = \frac{K_I^c}{K_{0I}^c}, \tag{2.69}$$

where K_{0I}^{a} is the mode I stress intensity factor at $x = a$ due to the presence of a central crack only, and K_{0I}^{b} and K_{0I}^{c} are the stress intensity factors at $x = b$ and $x = c$, respectively, due to the presence of outer cracks only.

2.6 Results and discussion

In this section, the goal is to find the temperature field, thermal tangential and normal stresses, SIFs, and SMFs for different particular cases of thermal loading, mechanical loading, and thermo-mechanical loading. The main interest of the present study is to investigate the interactions between a central crack and two symmetrically situated collinear cracks in an infinite functionally graded medium under thermo-mechanical loading.

During numerical computation, fixed negative values of the parameters δ, β, and γ are chosen. The reason for selecting negative values for these parameters is that that when the FGM is utilized for thermal shielding purpose, the upper face of the medium $y \to \infty$ should be made of a heat-resistive material such as ceramic and the lower face $y \to -\infty$ should be made of a metallic-type material [8]. Also, N (the number of terms retained in the series expansion of auxiliary functions) will be increased until the repetition of four digits in the entire calculation appears. The normalizing parameters are chosen as $T_0 = Q_0/k_0$ and $w_0 = (\mu_0 Q_0 \alpha_0)/k_0$. The normalised SIFs are taken as $k_I^a = K_I^a/\left(p_0\sqrt{a}\right)$, $k_I^b = K_I^b/\left(p_0\sqrt{0.5(c-b)}\right)$ and $k_I^c = K_I^c/\left(p_0\sqrt{0.5(c-b)}\right)$.

2.6.1 Temperature field

Figures 2.2a and 2.2b depict the temperature distributions along $y = 0^+$ and $y = 0^-$ for different values of a and b, respectively. Both the figures are plotted for $\delta = -1$ and $k^* = 0.25$.

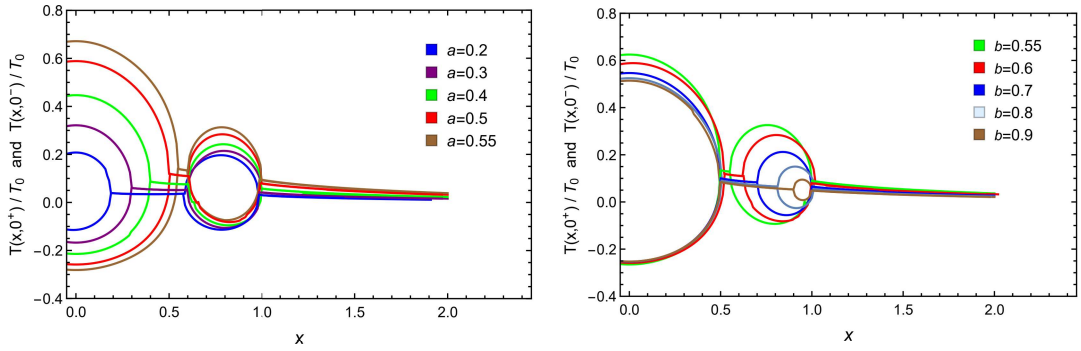

(a) **(b)**

Figure 2.2: Variations in normalized temperature field as a function of x for different values of (a) central crack tip a and (b) outer crack tip b.

Figure 2.2a illustrates the temperature distribution for fixed length of outer crack ($b = 0.6, c = 1$) and varying length of the central crack ($a = 0.2(0.1)0.5, 0.55$). In this case, the temperature distributions across the cracks become more pronounced. In Figure 2.2b central crack length is fixed ($a = 0.5$) and outer crack length is decreasing ($b = 0.55, 0.6(0.1)0.9$ and $c = 1$). The temperature across the cracks decreases in this case. Here, as the central crack approaches to the outer crack the temperature increases for both cracks, and when the outer crack goes away from the central crack and decreases its length, the temperature decreases for both cracks.

Note that the ratio Q_0/k_0 works as a scaling constant because temperature field T depends on the nonhomogeneity parameter δ and heat conductivity index k^*. It may also be noted that the temperature distribution is symmetric for the y-axis but asymmetric for the x-axis. This asymmetry of the x-axis is justified by

the fact that the heating source is generated from the upper half of the medium, and partially insulated cracks are working as heat barriers.

2.6.2 Thermal tangential and normal stresses

In the Figures 2.3 and 2.4, the distributions of thermal tangential and normal stresses are plotted for different values of a and b, respectively. The figures are plotted for $\delta = -1$, $\beta = -1$, $\gamma = -1$ and $k^* = 0.25$. The results are calculated under plane strain conditions and for the Poisson's ratio $v = 0.3$.

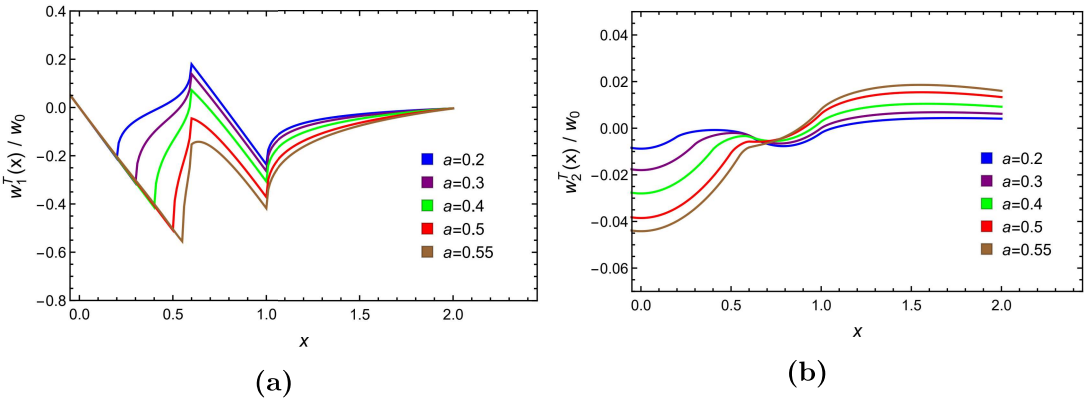

Figure 2.3: Variations in (a) normalized tangential stress and (b) normalized normal stress as a function of x for different values of central crack tip a.

From the Figures 2.3a and 2.3b, it may be observed that for the values of a $(a = 0.2(0.1)0.5, 0.55)$ while keeping b $(b = 0.6)$ and c $(c = 1)$ fixed there will be increasing tendencies in the thermal tangential and normal stresses for both central as well as outer cracks. This implies that when the central crack approaches to the outer crack both $w_1^T(x)$ and $w_2^T(x)$ increase. Figures 2.4a and 2.4b illustrate that for increasing values of b $(b = 0.55, 0.6(0.1)0.9)$ while keeping a $(a = 0.5)$ and c $(c = 1)$ fixed, the thermal tangential stress for outer crack tends to decrease but for

the central crack it remains almost unaffected. In this case, thermal normal stresses decrease for both the cracks.

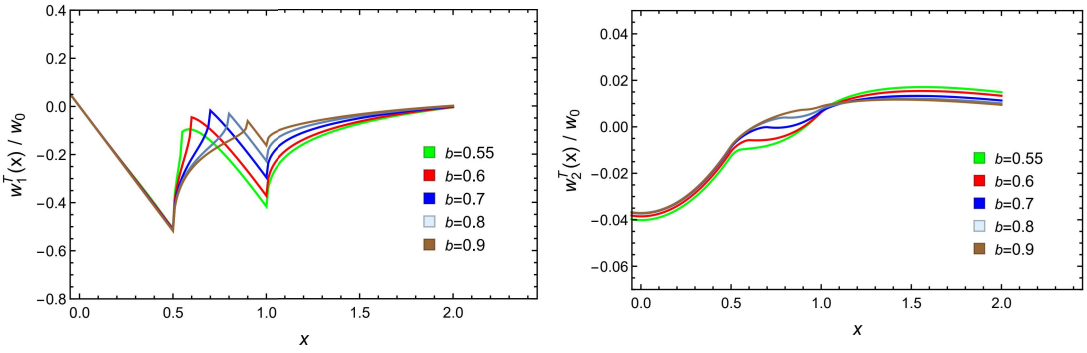

(a) **(b)**

Figure 2.4: Variations in (a) normalized tangential stress and (b) normalized normal stress as a function of x for different values of outer crack tip b.

It may be further observed that for FGMs, the distributions of the thermal tangential and normal stresses become nonlinear. It is anti-symmetric for thermal tangential stress and symmetric for thermal normal stress. Also, the ratio $(\mu_0 Q_0 \alpha_0)/k_0$ works as a scaling constant because the thermal crack surface stresses depend on δ, β and γ.

2.6.3 Stress intensity factors and stress magnification factors

Here the SIFs and SMFs have been calculated for three different loading conditions viz., thermal loading conditions, mechanical loading conditions and both thermal and mechanical loading conditions for the parameters' values $\delta = -1$, $\beta = -1$, $\gamma = -1$, $v = 0.3$ and $k^* = 0.25$. These results are calculated under plane strain conditions. In some cases, the values of mode I crack tip stress intensity factors are

negative. This negativity indicates the contact of the crack faces over a certain part or entire length. Due to this contact, friction will increase and the transfer of heat across the crack faces will become easier. Thus, it causes a lowering of the thermal stress intensity factor. This is one of the objectives of developing FGM materials. The results of SIFs and SMFs are obtained by keeping central crack length fixed at $a = 0.5$ and varying the length of the outer crack choosing $b = 0.55, 0.6(0.1)0.9$ with $c = 1$. Those also can be found by keeping length of the outer crack fixed at $b = 0.6$, $c = 1$ and varying central crack length by choosing $a = 0.2(0.1)0.5, 0.55$.

2.6.3.1 Relevance of thermal loading

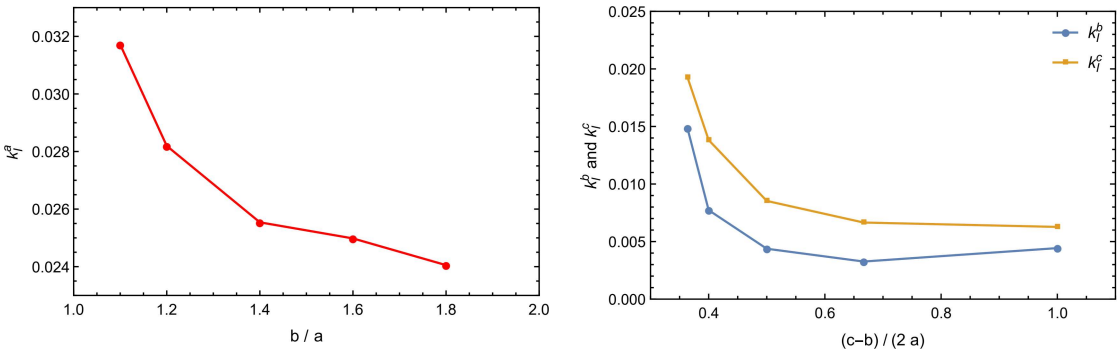

Figure 2.5: Plots showing normalised SIFs (a) at the central crack tip a as a function of normalized outer crack tip b/a and (b) at the outer crack tips b and c as a function of normalized central crack tip $(c-b)/(2a)$ subjected to thermal loading.

Figure 2.5a illustrates that as the length of the outer crack decreases, the normalized SIF at the crack tip a decreases under thermal loading. Whereas Figure 2.5b shows that as the length of central crack increases normalised SIFs at the crack tips b and c increase. It may be noticed that for the outer crack the values of the SIF of the outer crack tip are greater than the inner crack tip which is opposite to the case of collinear cracks' interactions in homogeneous materials. The reason for

this difference is due to the non-homogeneity of FGMs. These results show that under thermal loading when the two collinear cracks are approaching close to each other, the SIFs at the tips of the cracks increase.

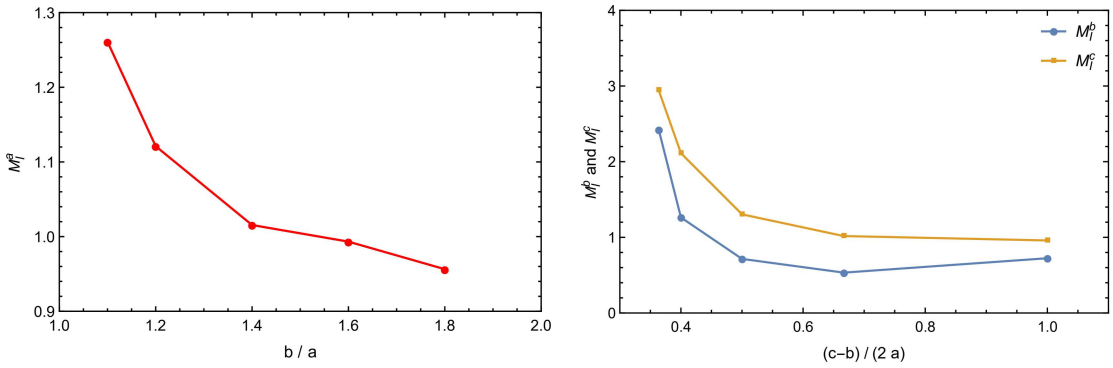

(a) **(b)**

Figure 2.6: Plots showing SMFs (a) at the central crack tip a as a function of normalized outer crack tip b/a and (b) at the outer crack tips b and c as a function of normalized central crack tip $(c-b)/(2a)$ subjected to thermal loading.

From Figure 2.6a, it is seen that as the length of the outer crack decreases, the SMF at the crack tip a decreases under thermal loading. Due to shielding ($M_{Ia} < 1$), there is a possibility of crack arrest. As the length of the outer crack increases the effect of shielding is changed to amplification ($M_{Ia} > 1$). Similarly, Figure 2.6b shows that when the length of the central crack increases the effect of shielding is changed to an amplification effect. Under this loading condition, the interaction effect is a mixture of amplification and shielding and when the distance between the cracks is greater than or equal to 0.2, there is the possibility of crack arrest.

2.6.3.2 Relevance of mechanical loading

In this section, SIFs and SMFs at the cracks' tips are discussed for two different mechanical loading conditions one for symmetric constant mechanical normal tractions and another for antisymmetric linearly distributed mechanical shear tractions.

For *symmetric constant mechanical normal tractions*, let us choose $w_1^M(x) = 0$ and

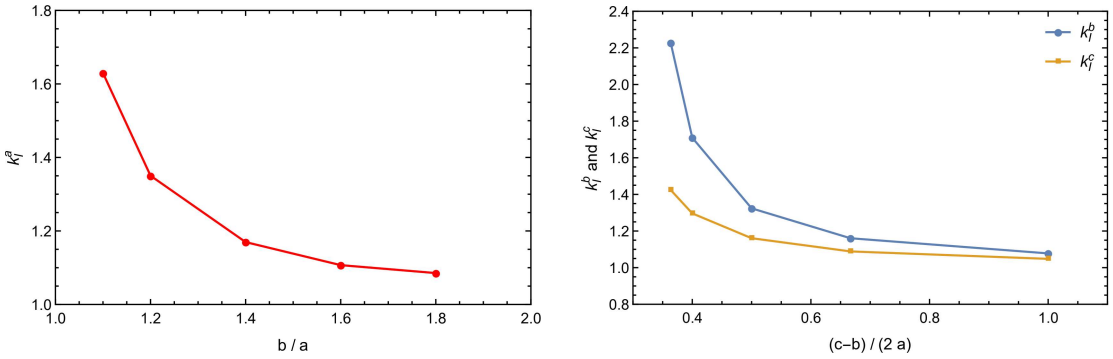

(a) **(b)**

Figure 2.7: Influence of constant mechanical normal traction on normalised SIFs (a) at the central crack tip a as a function of normalized outer crack tip b/a and (b) at the outer crack tips b and c as a function of normalized central crack tip $(c-b)/(2a)$.

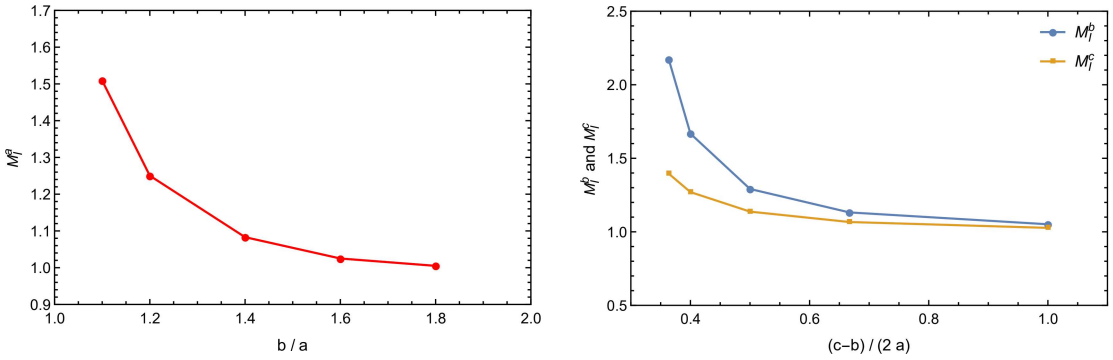

(a) **(b)**

Figure 2.8: Influence of constant mechanical normal traction on SMFs (a) at the central crack tip a as a function of normalized outer crack tip b/a and (b) at the outer crack tips b and c as a function of normalized central crack tip $(c-b)/(2a)$.

$w_2^M(x) = -p_0$. From Figure 2.7, it is seen that when the cracks are approaching close to each other, the SIFs at the cracks' tips are increasing. Here k_{Ib} is greater than k_{Ic} which is opposite to the case of thermal loading in which k_{Ib} is less than k_{Ic}. From Figure 2.8, it is seen that when the cracks are approaching close to each other, the SMFs at the cracks' tips are increasing and greater than or equal to 1. It indicates that there is no possibility of crack arrest since the amplification is observed under this mechanical loading condition.

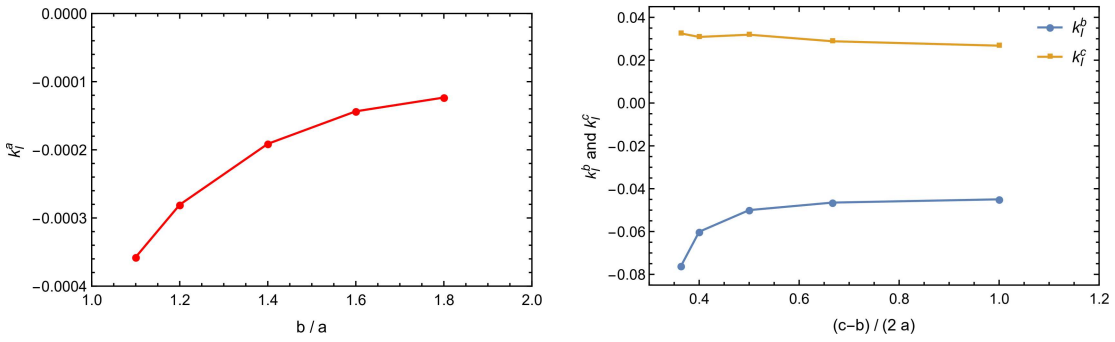

Figure 2.9: Influence of antisymmetric linearly distributed mechanical shear traction on normalised SIFs (a) at the central crack tip a as a function of normalized outer crack tip b/a and (b) at the outer crack tips b and c as a function of normalized central crack tip $(c-b)/(2a)$.

For *antisymmetric linearly distributed mechanical shear tractions*, let us choose $w_1^M(x) = -p_0 x$ and $w_2^M(x) = 0$. Under this loading condition it is observed from Figure 2.9 that the values of SIFs at the cracks' tips a and b are negative. In this loading condition, there may be the possibility of contact of crack faces either partially or completely. Further, it may be observed from Figure 2.9 that as the distance between the cracks is decreasing there is an absolute value increment in SIFs at the cracks' tips. Figure 2.10 illustrates that when the cracks are approaching close to each other, the SMFs are increasing. In this case, M_{Ia} and M_{Ib} are greater than 1 but M_{Ic} is less than 1 which indicates that the outer tip of the outer crack

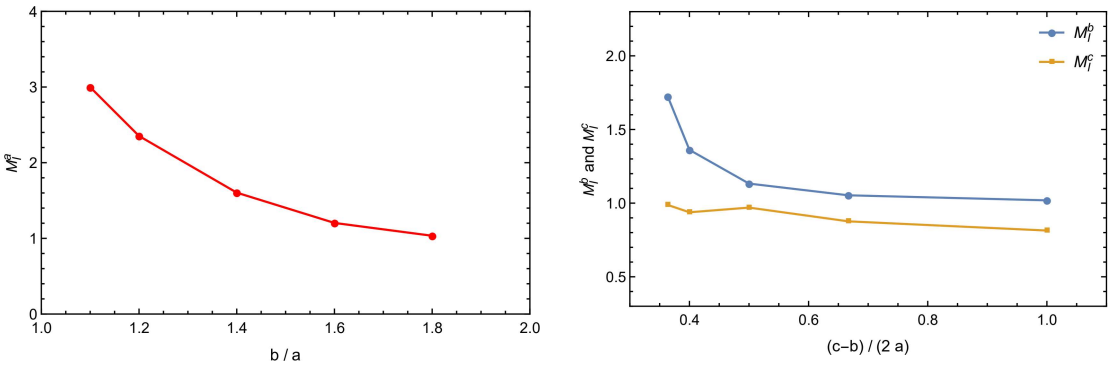

Figure 2.10: Influence of antisymmetric linearly distributed mechanical shear traction on SMFs (a) at the central crack tip a as a function of normalized outer crack tip b/a and (b) at the outer crack tips b and c as a function of normalized central crack tip $(c-b)/(2a)$.

experiences a shielding effect due to the presence of the central crack. This effect is maximum when the central crack size is small and the crack separation distance between central and outer cracks is large.

2.6.3.3 Relevance of thermo-mechanical loading

In this section, the interaction effects on the SIFs and SMFs are discussed under both thermal and mechanical loadings. To see the impact of both the loadings together, two mechanical loading conditions, as discussed in section 2.6.3.2, are chosen.

Figures 2.11 and 2.12 show the effects of variations of cracks' separation length on SIFs and SMFs, respectively, under the *thermal and symmetric constant mechanical normal tractions* ($w_1^M(x) = 0$ and $w_2^M(x) = -p_0$). In this combined loading condition, it is seen from Figure 2.11 and Figure 2.12 that as the length of the crack decreases the SIFs and SMFs decrease significantly. Individually in both cases, as observed from Figure 2.5 and Figure 2.7 that SIFs in the case of thermal loading are very small as compared to a symmetric constant mechanical

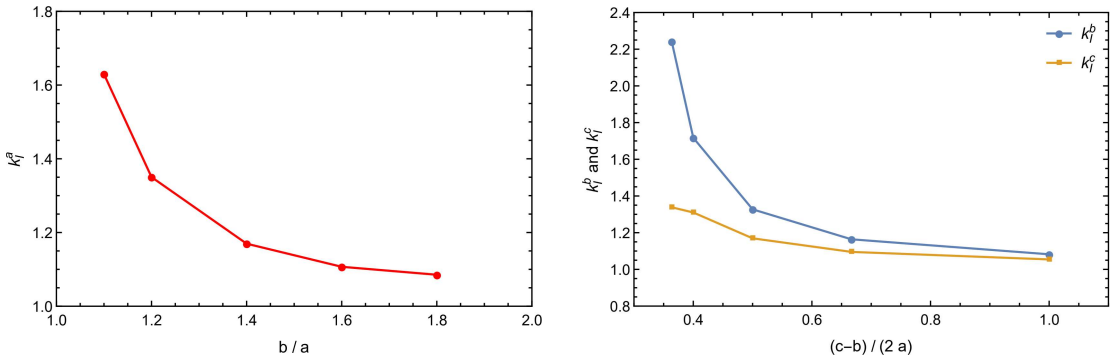

(a) **(b)**

Figure 2.11: Effect on normalised SIFs (a) at the central crack tip a as a function of normalized outer crack tip b/a and (b) at the outer crack tips b and c as a function of normalized central crack tip $(c-b)/(2a)$ subjected to thermal and symmetric constant mechanical normal traction.

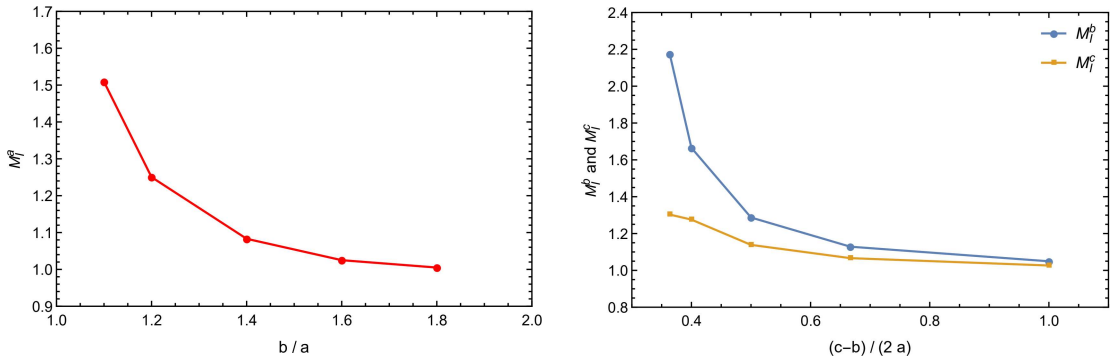

(a) **(b)**

Figure 2.12: Effect on SMFs (a) at the central crack tip a as a function of normalized outer crack tip b/a and (b) at the outer crack tips b and c as a function of normalized central crack tip $(c-b)/(2a)$ subjected to thermal and symmetric constant mechanical normal traction.

normal traction. Therefore, in the combined loading condition mechanical tractions dominate the thermal one, and SIFs and corresponding SMFs show similar behavior as obtained in the mechanical case with $k_{Ib} > k_{Ic}$ and there will be no possibility of crack arrest.

In the Figures 2.13 and 2.14, the effects of variations of length on the SIFs and SMFs, respectively, under *thermal and antisymmetric linearly distributed*

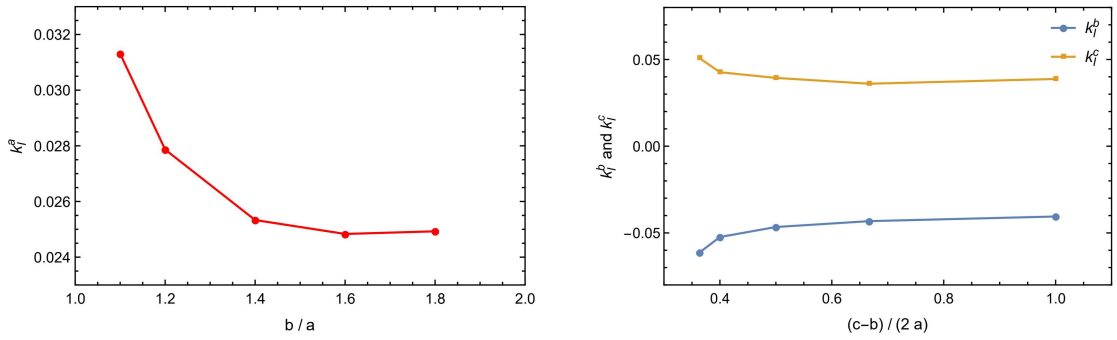

(a) **(b)**

Figure 2.13: Effect on normalised SIFs (a) at the central crack tip a as a function of normalized outer crack tip b/a and (b) at the outer crack tips b and c as a function of normalized central crack tip $(c-b)/(2a)$ subjected to thermal and antisymmetric linearly distributed mechanical shear traction.

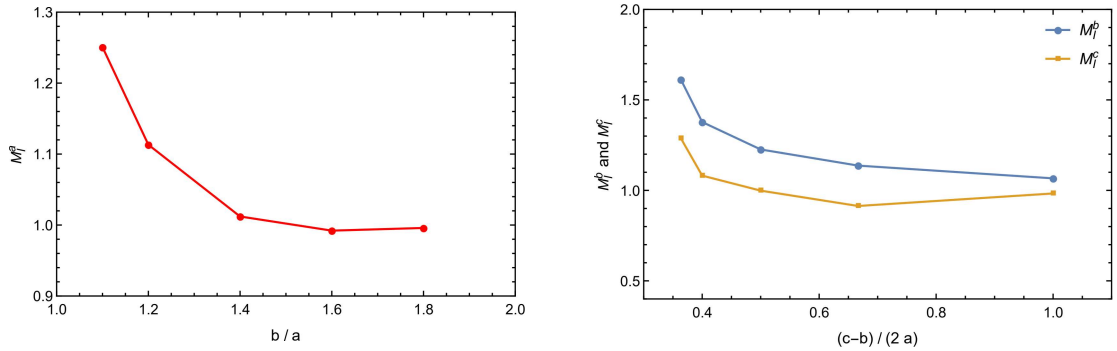

(a) **(b)**

Figure 2.14: Effect on SMFs (a) at the central crack tip a as a function of normalized outer crack tip b/a and (b) at the outer crack tips b and c as a function of normalized central crack tip $(c-b)/(2a)$ subjected to thermal and antisymmetric linearly distributed mechanical shear traction.

mechanical shear tractions ($w_1^M(x) = -p_0 x$ and $w_2^M(x) = 0$) are shown. Under this combined loading condition, it may be observed from the figures that as the length of the crack decreases, the SIFs and SMFs decrease in absolute values. In this case, k_{Ib} negative is indicating that there is the possibility of partial or complete contact with cracks' faces. Also, from Figure 2.14 it is noticed that there are possibilities of crack arrest at the cracks' tips a and c. Under this loading condition, the interaction effect is the combination of both crack shielding and amplification. As the distance

between the cracks is greater than 0.2, there is a possibility of crack arrest. It may be observed from the above results that stress at the tips increases under the influences of both thermal and mechanical loadings.

2.7 Concluding remarks

This chapter aims to advance understanding of the behavior of SIFs and the potential for crack arrest and crack propagation caused by interactions between partially insulated Griffith cracks with one central and two symmetrically positioned collinear Griffith cracks in an infinite functionally graded medium subject to thermo-mechanical loading. The following four key objectives were accomplished in this study:

1. The temperature field, thermal crack surface stresses, and mode I SIFs and SMFs expressions at the crack tips for the problem under consideration are found.

2. The pictorial presentations of the temperature field and thermal crack surface stresses show the increasing and decreasing tendencies when collinear cracks are moving in close proximity to one another and vice versa.

3. The graphical presentations of SIFs under different mechanical, thermal, and thermo-mechanical loading conditions demonstrate that SIFs rise in absolute value when collinear cracks are close to one another. There is also a possibility of cracks' closure in some cases.

4. The graphical presentations of shielding effects through the stress magnification factors help to find the possibility of crack arrest. The interaction effects

between the cracks can occasionally be either pure amplification or a combination of amplification and shielding.

****